


Correlation Hyperspectral Imaging

Gianlorenzo Massaro¹, Francesco V. Pepe^{1,*}, and Milena D'Angelo²
 Dipartimento Interateneo di Fisica, Università degli Studi di Bari, I-70126 Bari, Italy
 and Istituto Nazionale di Fisica Nucleare, Sezione di Bari, I-70125 Bari, Italy

 (Received 15 July 2024; revised 10 September 2024; accepted 10 October 2024; published 28 October 2024)

Hyperspectral imaging aims at providing information on both the spatial and the spectral distribution of light, with high resolution. However, state-of-the-art protocols are characterized by an intrinsic trade-off imposing to sacrifice either resolution or image acquisition speed. We address this limitation by exploiting light intensity correlations, which are shown to enable overcoming the typical downsides of traditional hyperspectral imaging techniques, both scanning and snapshot. The proposed approach also opens possibilities that are not otherwise achievable, such as sharper imaging and natural filtering of broadband spectral components that would otherwise hide the spectrum of interest. The enabled combination of high spatial and spectral resolution, high speed, and insensitivity to undesired spectral features shall lead to a paradigm change in hyperspectral imaging devices and open up new application scenarios.

DOI: [10.1103/PhysRevLett.133.183802](https://doi.org/10.1103/PhysRevLett.133.183802)

Spectral imaging has significantly contributed to fields such as material science, biology, and astronomy by providing detailed spatial and spectral information about the objects under study [1–4]. Spectral imaging techniques can be divided into two main categories: snapshot techniques, which are the fastest but suffer from a direct conflict between spatial and spectral resolution [5,6], and scanning techniques, which are slower due to a trade-off between resolution (either spatial or spectral) and acquisition time [1,2,7]. All traditional methods thus face limitations in resolution, sensitivity, and speed, strongly required to capture dynamic processes. A powerful alternative to conventional imaging techniques has emerged in the field of quantum imaging, where the statistical properties of light are exploited to offer new and unique advantages, such as overcoming the typical limitations of conventional devices [8–19]. Such correlation-based imaging approaches leverage the quantum and classical correlations of photons to extract information about the object. By analyzing the statistical relationships between light beams, these methods can enhance image resolution, improve signal-to-noise ratios, and enable imaging under conditions where conventional methods fail [20–33]. The underlying principle is that photons carry correlated information about the sample that can be decoded to reconstruct an image with enhanced features.

*Contact author: francesco.pepe@ba.infn.it

Published by the American Physical Society under the terms of the [Creative Commons Attribution 4.0 International license](https://creativecommons.org/licenses/by/4.0/). Further distribution of this work must maintain attribution to the author(s) and the published article's title, journal citation, and DOI.

In this Letter, we propose a novel approach to spectral imaging, based on light intensity correlation. This technique, named correlation hyperspectral imaging (CHI), can provide detailed spectral and spatial information about the sample, overcoming some of the downsides of both snapshot and scanning techniques. Furthermore, the use of correlations has several advantages not achievable with any other technique, such as the possibility of becoming insensitive to unwanted spectral features which overlap with the spectrum of interest, and improved optical performance enabled by light spatial coherence. These benefits make the proposed approach a promising tool for applications in biomedical imaging, where high resolution and efficiency are paramount, as well as environmental monitoring and industrial inspection, which would benefit from the loss of sensitivity to undesired spectral features, as well as by the combination of high resolution and fast acquisition.

In CHI, the combined spatial and spectral information required for spectral imaging is obtained by measuring the intensity on two separate sensors: light emitted by the sample is split into two optical arms, so that spatial information (i.e. the panchromatic intensity distribution) is retrieved by measuring light intensity on a monochrome imaging system, while the spectrum is measured through a dedicated spectrometer, as schematically reported in Fig. 1. The spectral image, which combines spectrum and spatial intensity distribution, is obtained by measuring the cross-correlation function between light intensity *fluctuations* at the two sensors

$$\Gamma(\boldsymbol{\rho}_a, \boldsymbol{\rho}_b, \Delta t) = \langle \Delta \bar{I}_a(\boldsymbol{\rho}_a, t) \Delta \bar{I}_b(\boldsymbol{\rho}_b, t + \Delta t) \rangle \quad (1)$$

where \bar{I}_a and \bar{I}_b are the 2D intensity distributions collected at the spatial (a) and spectral (b) sensors, $\Delta \bar{I}_i = \bar{I}_i - \langle \bar{I}_i \rangle$,

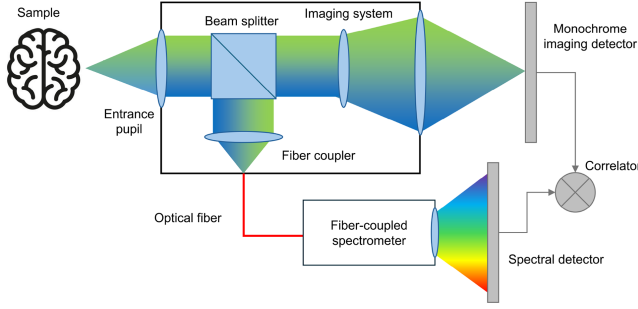


FIG. 1. Schematics of the experimental setup. The intensity fluctuations detected in time by the monochrome imaging sensor and the spectrometer are correlated to obtain a hyperspectral image of the sample.

with $i = a, b$ denotes the intensity fluctuations around its average value, ρ_a and ρ_b indicate the coordinates on the sensors surface, t represents the temporal coordinate, and Δt the correlation time delay. $\langle X \rangle$ denotes the statistical average of the stochastic quantity X . We shall assume the intensity from the sample to be stationary, so that the correlation function is independent of the time t and only depends on the time delay Δt . Though a 1D sensor array is generally sufficient for spectral detection, the availability of 2D arrays allows one to exploit redundancy of the collected intensity to improve the signal-to-noise ratio of the measurement at a given spectral frequency.

One of the key aspects of our technique is the ability to tune its spectral sensitivity to the statistical phenomena of interest. This can be seen by taking into account the finite bandwidth of the sensors, so that the quantity \bar{I}_i appearing in (1) is not the *instantaneous* light intensity distribution but the *time-averaged* intensity measured, at time t , by a detector with response time τ_{exp} , namely,

$$\bar{I}_i(\rho_i, t) = \frac{1}{\tau_{\text{exp}}} \int_t^{t+\tau_{\text{exp}}} |E_i(\rho_i, z_i, t')|^2 dt', \quad (2)$$

where z_i is the axial coordinate of detector $i = a, b$, and E_i is the electric field on its surface. The finite bandwidth of the detector is well known, in the context of correlation-based methods based on thermal light, to have detrimental effects on the measured correlation function. This is due to the fact that, as the detector response time τ_{exp} becomes larger than the light coherence time, intensity fluctuations are integrated and their relative amplitude tends to vanish ($\Delta \bar{I} / \langle \bar{I} \rangle \rightarrow 0$), making the evaluation of correlations more and more sensitive to noise. In the context of spectroscopy, however, one must consider that the overall spectrum is typically contributed by a plethora of different phenomena, each with its own features and bandwidth. These phenomena can mostly be considered to be *statistically independent* from one another, and, as such, each one characterized by its own coherence time. It is thus rather intuitive that, by appropriately setting the detector response time, the

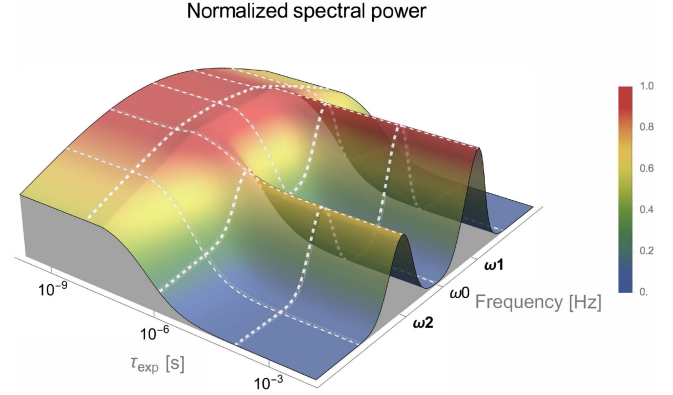


FIG. 2. CHI correlation function. Improvement of the spectral contrast for varying response time τ_{exp} , in the case of two narrow-band signals superposed to a broadband background.

multispectral correlation function can be adjusted to loose sensitivity to broadband spectral features, having a small coherence time, and isolate fluctuations due to the narrow-band emission of the phenomena of interest. This feature is very useful in many cases of interest for spectroscopy, where one is not interested in the known shape of broadband contributions (e.g. blackbody spectrum) but only to the line-shaped footprint of the material of interest.

To focus on this aspect, we shall now disregard the spatial features of the sample and only consider the spectrum originating from a single spatial coordinate on the sample. In Fig. 2, we report the simulated spectral part of the correlation function obtained by spanning a large range of detector response time; in the considered situation, three statistical phenomena coexist in a small portion of the object: a broadband (low-coherence) emission, centered at a frequency $\omega_0 = 100$ THz, characterized by a Gaussian spectrum having width $\Delta\nu_0 = 100$ GHz, and two narrow-band lines centered at $\omega_{1,2} = \omega_0 \pm 25$ GHz, both having bandwidth $\Delta\nu = 10$ kHz. The spectrum is measured through a spectrometer with resolution $\Delta\nu_{\text{spec}} = 10$ GHz, so that the perceived width of the narrow-line emission is defined by $\Delta\nu_{\text{spec}}$, although two narrow emissions can still be clearly resolved. To better highlight the usefulness of the *statistical filtering* operated by CHI through tuning of τ_{exp} (which can often be conveniently made by binning data in post processing), we choose to simulate a case where the emission of photons from the broadband emission is much more likely than the emission that contributes to the two lines. We thus fixed the photon flux to be 1000 times larger than the photon flux of the emission centered at ω_1 , and 1400 times larger than the emission centered at ω_2 . In these conditions, when the response time is small enough to be sensitive to the whole emission spectrum, the signal from the two lines is drowned in the uninteresting broadband background. Actually, since in the considered case $\Delta\nu \ll \Delta\nu_{\text{spec}} \ll \Delta\nu_0$, when $\tau_{\text{exp}} \ll (\Delta\nu_0)^{-1}$, the contrast between the most intense line and the broadband maximum is

$$C_0 \simeq \left(\frac{n}{n_0}\right)^2 \left(\frac{\Delta\nu_0}{\Delta\nu_{\text{spec}}}\right)^2 = 10^{-4}, \quad (3)$$

with $n/n_0 = 10^{-3}$ the ratio between the photon fluxes. As clearly demonstrated in Fig. 2, the increase in response time suppresses the broadband background much more than it does on the line-width emission; the highest possible contrast is obtained for $\tau_{\text{exp}} \gg (\Delta\nu)^{-1}$, and reads

$$C_\infty \simeq \left(\frac{n}{n_0}\right)^2 \frac{\Delta\nu_0}{\Delta\nu_{\text{spec}}} \frac{\Delta\nu_0}{\Delta\nu} = 10^2. \quad (4)$$

Large response times, which are typically detrimental in correlation measurements, result, in CHI, in a six-order of magnitude increase of the contrast of narrow lines over the useless broadband emission, as determined by the ratio $C_\infty/C_0 = \Delta\nu_{\text{spec}}/\Delta\nu$. In correlation-based spectroscopy, the increase of the detector response time thus boosts the spectral contrast. This feature is completely absent in conventional approaches, where detector integration time is typically adjusted to match the timescale of the investigated dynamical process, or, for slower processes, is increased for compensating for reduced sensitivity and improving the signal-to-noise ratio. On the contrary, in CHI, as long as the statistical fluctuations from background noise occur at a much faster rate than the slow dynamics of interest, larger response times only impact the spectral domain while leaving unchanged the time domain properties of the measurement. The reverse problem of discarding *narrowband* spurious components from the collected light is easily addressed by directly operating in the frequency domain; in our case, this is accomplished by simply discarding the pixels of the spectral detector corresponding to the given frequency to be removed.

After focusing the discussion on the characteristics of the pure spectral measurement, let us now focus on the features of the correlation function that determine the quality of the spatial image. For the sake of a lighter formalism, we shall now assume that the detectors are ideal ($\tau_{\text{exp}} = 0$), and only consider the x component of the 2D coordinates at the detector $\rho_{a,b} = (x_{a,b}, y_{a,b})$. The last assumption does not affect the spectral part of the measurement, since chromatic dispersion in spectrometers always occurs in one dimension (here chosen as x_b); it simply reduces the spatial detector to a pixel strip, limiting the analysis to *linear* images. For the sake of simplicity, we shall further assume that the correlation time delay is fixed at $\Delta t = (z_a - z_b)/c$, which compensates for the phase shift arising from the different optical paths leading to the two sensors and maximizes the visibility of the correlation function. In this simplified context, as shown in the Supplemental Material [34], (1) can be written as

$$\Gamma(x_a, \tilde{\omega}(x_b)) = \left| \int \int \tilde{I}(x_0, \omega) \tilde{g}_a^*(x_0, x_a) \tilde{g}_b(x_b, \omega) dx_0 d\omega \right|^2, \quad (5)$$

where $\tilde{I}(x_0, \omega)$ is the emission spectrum of the sample, as a function of the emission coordinate x_0 on the sample plane; the two functions $g_{a,b}$ represent the point-spread function (PSF) propagating the electric field from the sample plane to the spatial and spectral detector, respectively. Hence, the combined spatial and spectral information encoded within the correlation function is inherited by the properties of g_a and g_b , the former describing full-spectrum electromagnetic propagation through an imaging device, the latter describing propagation through a spectrometer, without any spatial information. Since the optical layout of the spectrometer arm is such to establish a correspondence between frequencies and detector coordinates, $x_b \rightarrow \tilde{\omega}(x_b)$, we chose to make this dependence explicit in the second argument of the correlation function. As per (5), the correlation function encoding the spectral image is a continuous superposition of *coherentlike* images: even though the imaging function is not sensitive to the phase of light on the sample, it still depends on the phase of the transfer functions; as recently demonstrated, such a property determines very distinctive features compared to standard *incoherent* images, such as very slow loss of focus and better resolution out of focus, both in intensity-based [35] and in correlation-based imaging [32].

To show the convenience of the coherentlike imaging capability of CHI, let us compare it with a typical frequency-sweeping technique. To this end, we shall consider the image obtained through the same imaging system of arm a , upon isolating a single frequency by means of a filter centered around ω' and bandwidth $\delta\nu_f$; of course, the acquisition of the complete spectral image requires that the center frequency of the filter sweeps the whole spectral range of interest. By modeling the filter frequency response through a positive function $\tilde{f}(\omega' - \omega)$, peaked around ω' and vanishing outside of the bandwidth, the obtained spectral image is

$$I_{\text{sw}}(x_a, \omega') = \int \tilde{I}(x_0, \omega) |\tilde{g}_a(x_0, x_a)|^2 \tilde{f}(\omega' - \omega) dx_0 d\omega. \quad (6)$$

Equations (5) and (6) are very similar: The imaging device described by g_a and the spectral device (described by either g_b or f) play the same role, giving rise to separate convolutions with the spatial and frequency dependence of \tilde{I} . The similarities are even more marked by selecting a filter bandwidth that matches the bandwidth of the spectrometer, namely $f(\omega' - \omega) = |\tilde{g}_b(x_b(\omega'), \omega)|^2$. Even if the optical and spectral performance are evenly matched in the two cases under inspection, so that the same exact functions are involved in the two equations, the key difference in the image formation process remains: in fact, standard techniques rely on an *incoherent* formation process, as determined by all positive-valued PSF appearing in (6), whereas the measurement of the correlation function results in a coherentlike superposition, as determined by the complex functions appearing in (5).

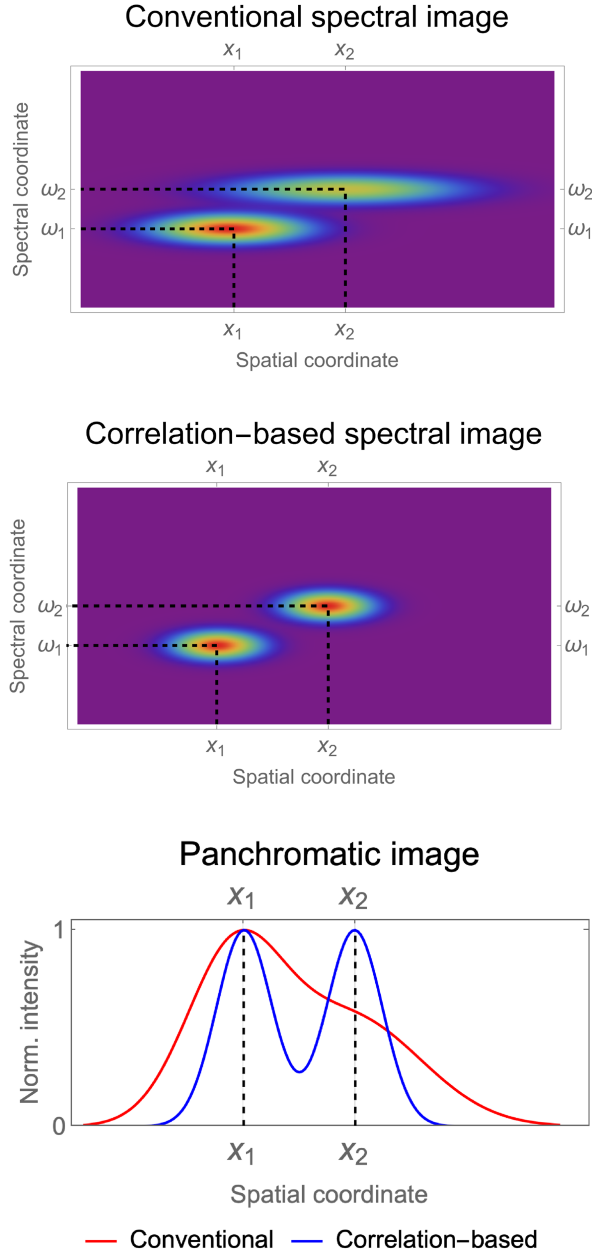


FIG. 3. Comparison between the optical performance of conventional sweeping hyperspectral imaging (top) and CHI (middle). Bottom: panchromatic image obtained through integration in frequency.

This can clearly be seen in Fig. 3, showing the optical performance advantage of the coherentlike spectral image encoded in the correlation function of CHI, over the (incoherent) image obtained through frequency sweeping. The simulation reports the spectral images of a sample consisting of two statistically independent emitters; both sources emit a Gaussian spectrum, centered at frequencies ω_1 and ω_2 , respectively. In order to compare the techniques as fairly as possible, the frequency filter and the spectrometer response have been set to be equal, Gaussian-shaped, with bandwidth $\Delta\nu_{\text{spec}} = \Delta\nu_f = |\omega_2 - \omega_1|/\pi$ matched to

$(\omega_2 - \omega_1)/\pi$, where $\omega_{1,2}$. We have chosen $\omega_1 = 100$ THz and $\omega_2 = \omega_1 + 50$ GHz. Each of the two statistical emissions from the sample is characterized by a very small bandwidth, so that their spectral image is defined by the filter-spectrometer resolution. Spatial information for the two cases is measured through the same imaging device: a 4-f system made of two identical lenses, placed at twice their focal length from each other, composed of two 50-mm lenses; the entrance pupil has a 0.2 numerical aperture, with Gaussian apodization for ease of calculation. In a 4-f system, a perfectly focused image is retrieved by the image sensor when the sample is in the first focal plane of the first lens. It is well known that a large-aperture (incoherent) imaging system can only retrieve a sharp image in close proximity of the focus; the image features undergo severe blurring upon moving away from the focus. On the contrary, coherentlike imaging gives rise to a much longer depth of field, regardless of the numerical aperture [35]. As demonstrated in Fig. 3, the coherentlike nature of CHI thus implies a significant advantage when the two sources emitting at ω_1 and ω_2 are not put in perfect focus. In the presented simulation, the two sources are identical: Gaussian-shaped, with a width of 1 mm, centered at $x_{1,2} = \pm 2$ mm, respectively, but are defocused by +1 cm and -1 cm, respectively (negative defocusing indicating an axial displacement toward the entrance pupil, and vice versa). Comparison between the upper and middle panels of Fig. 3 shows that the spectral properties of the two techniques (vertical axes) are identical, in accordance to our choice of matching the filter and spectrometer performance. However, the difference in imaging performance between the two hyperspectral imaging modalities is immediately evident: images from conventional hyperspectral imaging are blurred by the circle of confusion, and are thus much less localized than in CHI.

This is particularly evident by considering the panchromatic images obtained by integrating over the whole spectrum, as reported in the bottom plot of Fig. 3. We should also remark that, the conventional (*incoherent*) information is always available in CHI: the imaging arm, alone, gives the monochromatic (*incoherent*) image, and the spectral arm the emission spectrum. Most interestingly, CHI gives a panchromatic image by integrating the correlation function over frequency; such a correlation-based image has a much larger depth of field than the correlation-free (i.e., intensity-based) image: the very different nature of the two imaging modalities keeps showing up even when spectral features are neglected. In the Supplemental Material [34], we show a case in which the improved depth of field characterizing coherent imaging can be advantageous in a case of practical interest, namely, when one needs to spatially resolve a collection of possibly overlapping emitters, all characterized by the same spectrum, as is customary, for instance, with markers used in biomedical imaging applications.

In the example of Fig. 2, we have considered a physical regime in which the condition of isochronous detection [$\Delta t = (z_a - z_b)/c$] is approximately satisfied for the whole sample, regardless of the position of details on the optical axis. This situation is perfectly acceptable in CHI, thanks to the phase sensitivity of the correlation function and its connected coherentlike imaging behavior, which makes CHI capable of collecting a focused image of the whole sample, even with a modest numerical aperture. On the contrary, conventional techniques based on *incoherent* imaging yield a blurred image. This advantage of CHI is envisioned to be particularly useful in scenarios such as industrial inspection, when one wants to obtain a high-resolution spectral image with as much depth of field as possible, disregarding the details about the precise axial placement of the sample features.

Apart from the peculiar features of CHI so far discussed, the proposed approach has the further advantage of overcoming the intrinsic limitations of both scanning and snapshot hyperspectral imaging techniques. Snapshot techniques are based on the simultaneous measurement, on a single sensor, of both the spectrum and the image of the sample, and are typically achieved by mounting spectral filters on a conventional camera; each element of the image is thus observed at different frequencies. This approach entails a spatial resolution loss that is *at least* equal to the number of measured chromatic components. For instance, a Bayer matrix typically used in RGB imaging entails a loss of resolution by a factor four. Nonsnapshot, also known as scanning, techniques retrieve the spectral cube by acquiring one of its three dimensions over time: A single snapshot can be either a 2D image at a single frequency, so that the chromatic component is obtained by frequency-scanning (e.g., with a series of filters), or a linear image along with its spectrum, in which case the other axis is acquired by spatially scanning the sample along the remaining dimension. Thanks to the use of two disjoint sensors simultaneously collecting spatial and spectral information, CHI can acquire the spectral cube without being intrinsically subject to any such trade-off, thus enabling combining high spatial and spectral resolution, with high acquisition speed.

Another disadvantage of conventional hyperspectral imaging is its intrinsically wasteful nature of photons emitted by the sample. This is true for both snapshot techniques, where most of the optical intensity is lost because of frequency filtering, and scanning techniques, where one is only sensitive to a small portion of the object or its spectrum, at any given time. Conversely, the peculiar CHI decoupling of spatial and spectral measurement makes use of the entirety of the photons emitted by the object, possibly limited only by a finite angular acceptance of the device and optical losses.

In summary, correlation-based hyperspectral imaging represents a significant advancement in the field of spectral imaging. By utilizing the inherent statistical properties of

light, CHI offers new possibilities for high-resolution, sensitive, fast, and robust imaging across a wide range of applications. As research and technology in this area continue to advance, correlation-based imaging is expected to play a crucial role in addressing some of the most challenging problems of both snapshot and scanning conventional methods.

The analogy in the working principles of CHI and correlation 3D imaging [33,36–38] suggests the possibility of merging the two techniques, possibly at the expense of resorting to higher-order correlation functions.

In this regard, it is worth emphasizing that the working principle of CHI does not rely on specific characteristics tied to a particular frequency range, such as the infrared emission considered in the reported simulations. In fact, the frequency range and image quality of CHI will only be defined by the choice of optical components and detectors (e.g., by the frequency response of detectors and optics), while the type of samples and spectral ranges of applicability are basically the same as in conventional non-spatially resolving spectroscopy.

Further research will be dedicated to optimize the technique in terms of information content; in fact, despite being a fast and computationally feasible tool, the cross-correlation evaluation is not necessarily the optimal tool to extract the information contained in the raw datasets collected by the spatial and spectral detectors. This analysis shall also be combined to the study (e.g., through Fisher information) of the “photon efficiency” of the proposed scheme; here, we shall limit ourselves to highlight a very intuitive advantage offered by our approach over filtering or sweeping techniques: even upon severe statistical filtering (hence, information loss), our scheme still maintains the capability, at least in principle, to collect and process all incoming photons, thus leading to a significantly higher photon efficiency.

Acknowledgments—M. D. and F. V. P. acknowledge support by PNRR MUR Project No. PE0000023-NQSTI (National Quantum Science and Technology Institute). The activity is synergic to projects QuaASiModo, financed by the MUR Dipartimenti di Eccellenza '23-'27, and QUISS, financed by INFN.

-
- [1] H. F. Grahn and P. Geladi, *Techniques and Applications of Hyperspectral Image Analysis* (John Wiley & Sons, New York, 2007).
 - [2] D. Landgrebe, Information extraction principles and methods for multispectral and hyperspectral image data, in *Information Processing for Remote Sensing*, edited by C. H. Chen (World Scientific Publishing Company, River Edge, NJ, 1999), pp. 3–38.
 - [3] G. Vane, J. E. Duval, and J. B. Wellman, Imaging spectroscopy of the earth and other solar system bodies, in *Remote Geochemical Analysis: Elemental and Mineralogic*

- Composition*, edited by C. M. Pieters and P. A. J. Englert (Cambridge University Press, Cambridge, England, 1993), pp. 121–143.
- [4] G. Lu and B. Fei, Medical hyperspectral imaging: A review, *J. Biomed. Opt.* **19**, 010901 (2014).
- [5] N. Hagen, R. T. Kester, L. Gao, and T. S. Tkaczyk, Snapshot advantage: A review of the light collection improvement for parallel high-dimensional measurement systems, *Opt. Eng. (Bellingham, Wash.)* **51**, 111702 (2012).
- [6] N. Hagen and M. W. Kudenov, Review of snapshot spectral imaging technologies, *Opt. Eng. (Bellingham, Wash.)* **52**, 090901 (2013).
- [7] N. Gat, Imaging spectroscopy using tunable filters: A review, *Proc. SPIE Int. Soc. Opt. Eng.* **4056**, 50 (2000).
- [8] T. B. Pittman, Y.-H. Shih, D. V. Strekalov, and A. V. Sergienko, Optical imaging by means of two-photon quantum entanglement, *Phys. Rev. A* **52**, R3429 (1995).
- [9] M. Genovese, Real applications of quantum imaging, *J. Opt.* **18**, 073002 (2016).
- [10] P.-A. Moreau, E. Toninelli, T. Gregory, and M. J. Padgett, Imaging with quantum states of light, *Nat. Rev. Phys.* **1**, 367 (2019).
- [11] M. Gilaberte Basset, F. Setzpfandt, F. Steinlechner, E. Beckert, T. Pertsch, and M. Gräfe, Perspectives for applications of quantum imaging, *Laser Photonics Rev.* **13**, 1900097 (2019).
- [12] A. Valencia, G. Scarcelli, M. D’Angelo, and Y. Shih, Two-photon imaging with thermal light, *Phys. Rev. Lett.* **94**, 063601 (2005).
- [13] A. Gatti, E. Brambilla, M. Bache, and L. A. Lugiato, Ghost imaging with thermal light: Comparing entanglement and classical correlation, *Phys. Rev. Lett.* **93**, 093602 (2004).
- [14] F. Ferri, D. Magatti, A. Gatti, M. Bache, E. Brambilla, and L. A. Lugiato, High-resolution ghost image and ghost diffraction experiments with thermal light, *Phys. Rev. Lett.* **94**, 183602 (2005).
- [15] G. Scarcelli, V. Berardi, and Y. Shih, Can two-photon correlation of chaotic light be considered as correlation of intensity fluctuations?, *Phys. Rev. Lett.* **96**, 063602 (2006).
- [16] M. D’Angelo, A. Mazzilli, F. V. Pepe, A. Garuccio, and V. Tamma, Characterization of two distant double-slits by chaotic light second-order interference, *Sci. Rep.* **7**, 2247 (2017).
- [17] A. Chiuri, F. Angelini, S. Santoro, M. Barbieri, and I. Gianani, Quantum ghost imaging spectrometer, *ACS Photonics* **10**, 4299 (2023).
- [18] A. Chiuri, M. Barbieri, I. Venditti, F. Angelini, C. Battocchio, M. G. A. Paris, and I. Gianani, Fast remote spectral discrimination through ghost spectrometry, *Phys. Rev. A* **109**, 042617 (2024).
- [19] S. Mukamel *et al.*, Roadmap on quantum light spectroscopy, *J. Phys. B* **53**, 072002 (2020).
- [20] R. Meyers, K. S. Deacon, and Y. Shih, Ghost-imaging experiment by measuring reflected photons, *Phys. Rev. A* **77**, 041801(R) (2008).
- [21] N. D. Hardy and J. H. Shapiro, Ghost imaging in reflection: Resolution, contrast, and signal-to-noise ratio, *Proc. SPIE Int. Soc. Opt. Eng.* **7815**, 78150L (2010).
- [22] K. W. C. Chan, M. N. O’Sullivan, and R. W. Boyd, Two-color ghost imaging, *Phys. Rev. A* **79**, 033808 (2009).
- [23] D. Duan, Z. Man, and Y. Xia, Non-degenerate wavelength computational ghost imaging with thermal light, *Opt. Express* **27**, 25187 (2019).
- [24] S. Karmakar and Y. Shih, Two-color ghost imaging with enhanced angular resolving power, *Phys. Rev. A* **81**, 033845 (2010).
- [25] D. Kalashnikov, A. Paterova, S. Kulik, and L. A. Krivitsky, Infrared spectroscopy with visible light, *Nat. Photonics* **10**, 98 (2016).
- [26] A. V. Paterova, S. M. Maniam, H. Yang, G. Greci, and L. A. Krivitsky, Hyperspectral infrared microscopy with visible light, *Sci. Adv.* **6**, eabd0460 (2020).
- [27] R. E. Meyers, K. S. Deacon, and Y. Shih, Turbulence-free ghost imaging, *Appl. Phys. Lett.* **98**, 111115 (2011).
- [28] D. Shi, C. Fan, P. Zhang, J. Zhang, H. Shen, C. Qiao, and Y. Wang, Adaptive optical ghost imaging through atmospheric turbulence, *Opt. Express* **20**, 27992 (2012).
- [29] M. Bina, D. Magatti, M. Molteni, A. Gatti, L. A. Lugiato, and F. Ferri, Backscattering differential ghost imaging in turbid media, *Phys. Rev. Lett.* **110**, 083901 (2013).
- [30] B. Sun, M. P. Edgar, R. Bowman, L. E. Vittert, S. Welsh, A. Bowman, and M. J. Padgett, 3D computational imaging with single-pixel detectors, *Science* **340**, 844 (2023).
- [31] M. D’Angelo, F. V. Pepe, A. Garuccio, and G. Scarcelli, Correlation plenoptic imaging, *Phys. Rev. Lett.* **116**, 223602 (2016).
- [32] F. V. Pepe, F. Di Lena, A. Mazzilli, E. Edrei, A. Garuccio, G. Scarcelli, and M. D’Angelo, Diffraction-limited plenoptic imaging with correlated light, *Phys. Rev. Lett.* **119**, 243602 (2017).
- [33] G. Massaro, P. Mos, S. Vasiukov, F. Di Lena, F. Scattarella, F. V. Pepe, A. Ulku, D. Giannella, E. Charbon, C. Bruschini, and M. D’Angelo, Correlated-photon imaging at 10 volumetric images per second, *Sci. Rep.* **13**, 12813 (2023).
- [34] See Supplemental Material at <http://link.aps.org/supplemental/10.1103/PhysRevLett.133.183802> for additional theoretical details that corroborate the arguments presented in the main text.
- [35] G. Massaro, B. Barile, S. Giuliano, F. V. Pepe, G. P. Nicchia, and M. D’Angelo, Direct 3D imaging through spatial coherence of light, *Laser Photonics Rev.* **18**, 2301155 (2024).
- [36] C. Abbattista *et al.*, Towards quantum 3D imaging devices, *Appl. Sci.* **11**, 6414 (2021).
- [37] G. Massaro, F. Di Lena, M. D’Angelo, and F. V. Pepe, Effect of finite-sized optical components and pixels on light-field imaging through correlated light, *Sensors* **22**, 2778 (2022).
- [38] G. Massaro *et al.*, Light-field microscopy with correlated beams for high-resolution volumetric imaging, *Sci. Rep.* **12**, 16823 (2022).